Journal of Nuclear Materials 399 (2010) 181–188

Contents lists available at ScienceDirect

Journal of Nuclear Materials

journal homepage: www.elsevier.com/locate/jnucmat

First-principles study of ground-state properties and high pressure behavior of ThO_2

Bao-Tian Wang [a,b], Hongliang Shi [b,c], Wei-Dong Li [a], Ping Zhang [b,*]

[a] Institute of Theoretical Physics and Department of Physics, Shanxi University, Taiyuan 030006, People's Republic of China
[b] LCP, Institute of Applied Physics and Computational Mathematics, P.O. Box 8009, Beijing 100088, People's Republic of China
[c] State Key Laboratory for Superlattices and Microstructures, Institute of Semiconductors, Chinese Academy of Sciences, P.O. Box 912, Beijing 100083, People's Republic of China

ARTICLE INFO

Article history:
Received 18 November 2009
Accepted 19 January 2010

ABSTRACT

The mechanical properties, electronic structure and phonon dispersion of ground state ThO_2 as well as the structure behavior up to 240 GPa are studied using first-principles density-functional theory. Our calculated elastic constants indicate that both the ground-state fluorite structure and high pressure cotunnite structure of ThO_2 are mechanically stable. The bulk modulus, shear modulus, and Young's modulus of cotunnite ThO_2 are all smaller by approximately 25% compared with those of fluorite ThO_2. The Poisson's ratios of both structures are approximately equal to 0.3 and the hardness of fluorite ThO_2 is 22.4 GPa. The electronic structure and bonding nature of fluorite ThO_2 are fully analyzed, and show that the Th–O bond displays a mixed ionic/covalent character. The phase transition from the fluorite to cotunnite structure is calculated to occur at the pressure of 26.5 GPa, consistent with recent experimental measurement by Idiri et al. [1]. For the cotunnite phase it is further predicted that an isostructural transition takes place in the pressure region of 80–130 GPa.

1. Introduction

Besides uranium and plutonium, thorium is also an important nuclear material. Thorium metal and its compounds have been widely investigated both experimentally and theoretically since metal thorium was discovered in 1828. Among thorium compounds, thorium dioxide ThO_2, which is a stable diamagnetic transparent insulating solid, has attracted special attention. In addition to its usage as nuclear fuel material, thorium dioxide has also been used as a solid-state electrolyte. In particular, due to its prominent hardness, ThO_2 has potential interest as an optical component material and laser host.

Recently, a series of experimental reports on pressure-induced phase transition of ThO_2 [1–3] were reported in the literature. At ambient pressure, ThO_2 crystallizes in the (CaF_2-type) fluorite structure with space group $Fm\bar{3}m$ (No. 225). By using the energy dispersive X-ray diffraction method, Dancausse et al. [3] reported that at 40 GPa, ThO_2 undergoes a phase transition to the orthorhombic structure of cotunnite ($PbCl_2$) type with space group *Pnma* (No. 62). Later, through improved experimental measurement technique, Idiri et al. [1] observed that this phase transition really begins around 30 GPa, and that the two phases coexist in a wide pressure range of nearly 20 GPa. Additional high-pressure Raman spectroscopy measured by Jayaraman et al. [2] also suggested that ThO_2 starts to transform into the cotunnite structure at around 30 GPa.

In contrast to the above-mentioned extensive experimental investigations, only one theoretical study on the phase transition of ThO_2 at high pressure was reported recently by Boettger [4] who employing the relativistic linear combinations of Gaussian type orbitals-fitting function (LCGTO-FF) technique predicted a transition pressure of around 27.5 GPa. In addition, considering the obvious discrepancy between two works performed by one experimental group [1,3] involving the transition pressure, one more theoretical investigation from basis quantum mechanics is not only complementary but also indispensable. Motivated by this observation, in this paper, we present a first-principles study by calculating the total energies and enthalpies of ThO_2 at its experimentally established crystalline phases. Our calculation shows that the transition pressure is around 26.5 GPa, consistent with the recent experiment by Idiri et al. [1] and theoretical study by Boettger [4].

The other task for this paper is to theoretically present a thorough description of physical, mechanical and chemical bonding properties of ThO_2 at its ground state of the fluorite phase. To date, theoretical studies of the ground-state behavior of ThO_2 are very scarce in literature [5–11] and some of them are even inconsistent with the experimental data to a large extent. For example, without taking into account the 5f state, Kelly et al. [5] calculated the bulk modulus *B* of ThO_2 to be 290 GPa, which is far from the experimental value of 198 GPa. On the other hand, based on a purely ionic model, Harding et al. [6] obtained $B = 175$ GPa, which, compared to the experimental data, clearly underestimated the binding interaction in the material to a large extent. This as whole encourages us to theoretically report a systematic investigation on the

---

* Corresponding author. Tel.: +86 10 82305133.
E-mail address: zhang_ping@iapcm.ac.cn (P. Zhang).

0022-3115/$ - see front matter Crown Copyright © 2010 Published by Elsevier B.V. All rights reserved.
doi:10.1016/j.jnucmat.2010.01.017

ground-state properties of ThO_2 at its ambient phase. Besides the consistency with the existing experimental data, we expect that the new results for the first time predicted in this paper and experimentally inaccessible at present, such as the hardness, the phonon spectrum, and the charge transfer of the Th–O bond, will be of great help for a primary understanding of ThO_2. The rest of this paper is arranged as follows. In Section 2, the computational method is briefly described. In Sections 3 and 4, we present our calculated results, some of which are made comparison with available experimental and theoretical results. In Section 5, we summarize the conclusions of this work.

2. Computational method

Our total energy calculations are carried out by employing the plane-wave basis pseudopotential method as implemented in Vienna *ab initio* simulation package [12]. The exchange and correlation effects are described by the density-functional theory (DFT) within the generalized gradient approximation (GGA) [13]. The electron and core interactions are included using the frozen-core projected augmented wave approach which combines the accuracy of augmented-plane-wave methods with the efficiency of the pseudo-potential approach [14]. The thorium $6s^2 7s^2 6p^6 6d^1 5f^1$ and the oxygen $2s^2 2p^4$ electrons are treated as valence electrons. Note that although the 5f state are empty in elemental Th, this level evolves into a hybridization with O 2p state in the valence band, as well as contributes prominently to the conduction band (see Fig. 3 below). We use a $9 \times 9 \times 9$ k-point grid with Monkhorst–Pack scheme [15] for fluorite ThO_2 and $9 \times 15 \times 9$ k-point grid for cotunnite structure. The electron wave function is expanded in plane waves up to a cutoff energy of 500 eV, and all atoms are fully relaxed until the quantum mechanical forces become less than 0.02 eV/Å.

To obtain optimized lattice constants of ground state ThO_2, first, we calculated several total energies at different lattice constants around the experimental value. Then we fitted the energy-volume data to the third-order Birch–Murnaghan equation of state (EOS) [16] to give the theoretical equilibrium volume, minimum energy, bulk modulus B, and pressure derivative of the bulk modulus B'. On the other hand, the bulk modulus B, shear modulus G, Young's modulus E, Poisson's ratio υ, can also be derived from the elastic constants. We found that the bulk modulus B obtained by these two ways are in good agreement, indicating that our calculations are self-consistent. In order to investigate the high pressure behavior of ThO_2, we have optimized the structural parameters of its $Fm\bar{3}m$ and $Pnma$ phases at different pressures by using GGA method. To avoid the Pulay stress problem, we performed the structure relaxation calculations at fixed volumes rather than constant pressures. For $Fm\bar{3}m$ phase, due to its high symmetry, the structure relaxation calculations are performed at fixed volumes with no relaxation of coordinates. However, for $Pnma$ phase, the coordinates of atoms and the cell shape are necessary to be optimized due to their internal degrees of freedom.

3. Ground state properties for fluorite-type thorium dioxide

3.1. Atomic structure and mechanical properties

At ambient condition thorium dioxide crystallizes in a CaF_2-like ionic structure. Its cubic unit cell is composed of four ThO_2 formula units with the thorium atoms and the oxygen atoms in 4a and 8c sites, respectively (see Fig. 1a). Each Th atom is surrounded by eight O atoms forming a cube and each O connects with four Th atoms to build a tetragon. A particular feature of this structure is the presence of a large octahedral hole sited at position $(\frac{1}{2}, \frac{1}{2}, \frac{1}{2})$. The present optimized lattice constant (a_0) is 5.62 Å (see Table 1), in good agreement with the experimental [1,7] value of 5.6 Å.

Elastic constants can measure the resistance and mechanical features of crystal to external stress or pressure, thus describing the stability of crystals against elastic deformation. For small strains Hooke's law is valid and the crystal energy E is a quadratic function of strain [17]. Thus, to obtain the total minimum energy for calculating the elastic constants to second-order, a crystal is strained and all the internal parameters are relaxed. Consider a symmetric 3×3 nonrotating strain tensor $\boldsymbol{\varepsilon}$ which has matrix elements $\varepsilon_{ij}(i, j = 1, 2, \text{and } 3)$ defined by

$$\varepsilon_{ij} = \begin{pmatrix} e_1 & \frac{e_6}{2} & \frac{e_5}{2} \\ \frac{e_6}{2} & e_2 & \frac{e_4}{2} \\ \frac{e_5}{2} & \frac{e_4}{2} & e_3 \end{pmatrix}. \tag{1}$$

Such a strain transforms the three lattice vectors defining the unstrained Bravais lattice $\{\mathbf{a}_k, k = 1, 2, \text{and } 3\}$ to the strained vectors [18] $\{\mathbf{a}'_k\}$as defined by

$$\mathbf{a}'_k = (\mathbf{I} + \boldsymbol{\varepsilon})\mathbf{a}_k, \tag{2}$$

where $\mathbf{I}$ is a unit 3×3 matrix. Each lattice vector $\mathbf{a}_k$ or $\mathbf{a}'_k$ is a 3×1 matrix. The change in total energy due to above strain (1) is [17]

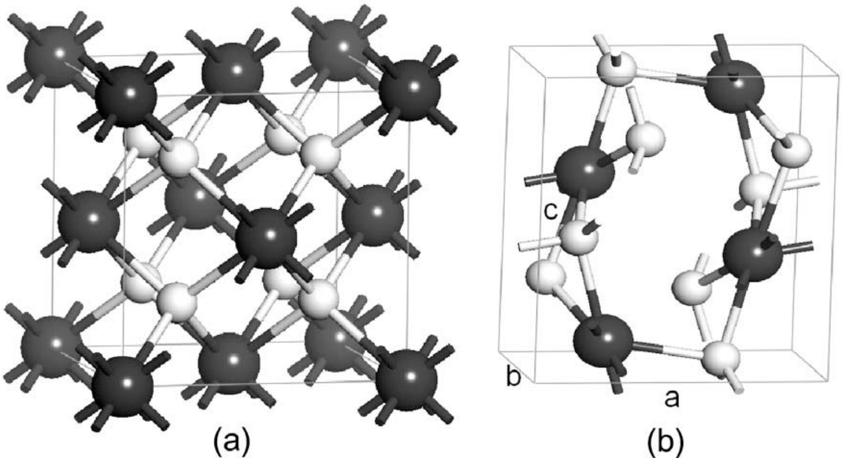

Fig. 1. Cubic unit cell for ThO_2 in space group $Fm\bar{3}m$ (a) and orthorhombic unit cell in space group $Pnma$ (b), larger black spheres stand for Th atoms and the smaller white O.

Table 1
Calculated lattice parameter, elastic constants, bulk modulus B, pressure derivative of the bulk modulus B', shear modulus G, Young's modulus E, Poisson's ratio υ, hardness, and energy band gap (E_g) for cubic ThO$_2$. As a comparison, other theoretical works and available experimental data are listed.

Property	This study	Previous calculation	Experiment
a_0 (Å)	5.62	5.61[a], 5.6225[b], 5.6257[c], 5.597[d]	5.60001(3)[e], 5.598(3)[g]
C_{11} (GPa)	349.5	376.0[a], 314.5[b]	367[f]
C_{12} (GPa)	111.4	109.8[a],73.1[b]	106[f]
C_{44} (GPa)	70.6	68.1[a], 75.7[b]	79[f]
B (GPa)	191	198[a], 192.8[b], 184.5[c], 198[g]	198(2)[e], 195(2)[g]
B'	4.5	4.5[a], 4.49[c], 4.2[g]	4.6(3)[e], 5.4(2)[g]
G (GPa)	87.1	94.1[a], 94.5[b]	97[f]
E (GPa)	226.8	243.8[a], 243.7[b]	249[f]
υ	0.302	0.295[a], 0.289[b]	0.285[f]
Hardness (GPa)	22.4		
E_g(eV)	4.673	4.60[b], 4.522[g]	6[h]

[a] Ref. [9].
[b] Ref. [10].
[c] Ref. [4].
[d] Ref. [11].
[e] Ref. [1].
[f] Ref. [19].
[g] Ref. [7].
[h] Ref. [26].

Table 2
Three strain combinations in the strain tensor [Eq. (1)] to calculate the three elastic constants of cubic ThO$_2$.

Strain	Parameters (unlisted $e_i = 0$)	$\Delta E/V$ in O (δ^2)
ϵ^1	$e_1 = \delta\ e_2 = \delta\ e_3 = \delta$	$\frac{3}{2}(C_{11} + 2C_{12})\delta^2$
ϵ^2	$e_1 = \delta\ e_3 = \delta$	$(C_{11} + C_{12})\delta^2$
ϵ^3	$e_4 = \delta\ e_5 = \delta\ e_6 = \delta$	$\frac{3}{2}C_{44}\delta^2$

$$\Delta E = E(V, \{\epsilon_i\}) - E(V, 0) = V\sum_{i=1}^{6}\sigma_i e_i + \frac{V}{2}\sum_{i,j=1}^{6} C_{ij}e_i e_j + O(\{e_i^3\}), \quad (3)$$

where $E(V,0)$ is the total energy for the unstrained crystal, σ_i are the elements of stress tensor, and C_{ij} are the elastic constants. For the cubic structure of ThO$_2$, there are three independent elastic constants, i.e., C_{11}, C_{12}, and C_{44}, which are calculated through a proper choice of the set of strains $\{e_i, i = 1, \ldots, 6\}$ listed in Table 2. In our first-principles calculations, the strain amplitude δ was varied in steps of 0.006 from δ=−0.036 to 0.036 and the total energies $E(V, \delta)$ at these strain steps were calculated, and then fitted through the strains with the corresponding parabolic equations of $\Delta E/V$ as given in Table 2 to yield the required second-order elastic constants. Note that while computing these energies all atoms are allowed to relax with the cell shape and volume fixed by the choice of strains $\{e_i\}$. Our calculated elastic constants for the ground-state fluorite structure of ThO$_2$ are listed in Table 1. As a comparison, previous theoretical results based on the full-potential linear muffin-tin orbital (FP-LMTO) method [9] and the full-potential linearized-augmented-plane-wave (FLAPW) method [4], as well as available experimental data [19] are also presented in Table 1. It is clear that our calculated elastic constants are in good agreement with the experimental results.

After obtaining the elastic constants, we can calculated the bulk and shear moduli from the Voigt–Reuss–Hill (VRH) approximations [20–22]. The Voigt bounds [20,23] on the effective bulk modulus B_V and shear modulus G_V are

$$B_V = (C_{11} + 2C_{12})/3 \quad (4)$$

and

$$G_V = (C_{11} - C_{12} + 3C_{44})/5. \quad (5)$$

Under Reuss approximation [21], the Reuss bulk modulus B_R and Reuss shear mudulus G_R are

$$B_R = B_V \quad (6)$$

and

$$G_R = 5(C_{11} - C_{12})C_{44}/[4C_{44} + 3(C_{11} - C_{12})]. \quad (7)$$

The bulk modulus B and shear modulus G, based on the Hill approximation [22], are arithmetic average of Voigt and Reuss elastic modulus, i.e., $B = \frac{1}{2}(B_R + B_V)$ and $G = \frac{1}{2}(G_R + G_V)$. The Young's modulus E and Poisson's ratio υ for an isotropic material are given by [24]

$$E = \frac{9BG}{3B + G}, \quad (8)$$

and

$$\upsilon = \frac{3B - 2G}{2(3B + G)}. \quad (9)$$

The calculated results for these moduli and Poisson's ratio for the fluorite ThO$_2$ are listed in Table 1. Note that we have also calculated the bulk modulus B by fitting the EOS. The derived bulk modulus turns out to be exactly the same as that from the above VRH approximation, which again indicates that our calculations are consistent and reliable. For comparison, other theoretical results [7,4,9] and available experimental data [1,7,19] are also shown in Table 1. It can be seen that on the whole, our present results compare well with those previous experimental and FP-LMTO/FLAPW theoretical results. Concerning the Poisson's ratio, it is well known that for the common materials that have much smaller shear moduli compared with the bulk moduli, their Poisson's ratio is close to 1/3. For the present ThO$_2$ system, our calculated shear modulus G is much lower than the bulk modulus B. Thus, our calculated result of 0.302 for the Poisson's ratio, as well as the derived result of 0.285 according to the experimentally determined elastic constants [19] and using Eq. (9), can be well understandable.

Furthermore, hardness is also one fundamental physical quantity when considering the phase stability and mechanical properties. Note that the hardness is important for the applications of ThO$_2$ as both nuclear material and optical components. So here we calculate the hardness of ThO$_2$ by using the approach raised by Simunek et al. [25]. In the case of two atoms 1 and 2 forming one bond of strength s_{12} in a unit cell of volume Ω, the expression for hardness has the form [25]

$$H = (C/\Omega)b_{12}s_{12}e^{-\sigma f_2}, \quad (10)$$

where

$$s_{12} = \sqrt{(e_1e_2)}/(n_1n_2d_{12}), \quad e_i = Z_i/r_i \quad (11)$$

and

$$f_2 = \left(\frac{e_1 - e_2}{e_1 + e_2}\right)^2 = 1 - \left[\sqrt{(e_1e_2)}/(e_1 + e_2)\right]^2 \quad (12)$$

are the strength and ionicity of the chemical bond, respectively, and d_{12} is the interatomic distance; C = 1550 and $\sigma = 4$ are constants. The radius r_i is chosen to make sure that the sphere centered at atoms i in a crystal contains exactly the valence electronic charge Z_i. For the fluorite structure of ThO$_2$, $b_{12} = 32$ counts the interatomic bonds between atoms Th (1) and O (2) in the unit cell, $n_1 = 8$ and $n_2 = 4$ are coordination numbers of atom Th and O, respectively, $r_1 = 1.81$ (Å) and r_2 = 1.00 (Å) are the atomic radii for Th and O atoms, respectively, $Z_1 = 12$ and $Z_2 = 6$ are valence charge for Th and O atoms, respectively, $d_{12} = 2.43$ (Å) is the interatomic distance, and $\Omega = 145.53$ (Å^3) is the volume of unit cell. Using Eqs. (10)–(12), we obtain $s_{12} = 0.081$ and $f_2 = 0.0025$. The hardness of ThO_2 at its ground-state fluorite structure is thus given by $H = 22.4$ (GPa). This indicates that the fluorite ThO_2 is a hard material and approaches to a superhard material (hardness > 40 GPa). The high hardness of this crystal can be understood from the dense crystal structure, which results in high valence electron density and short bond distances. The unusual mixture of covalent and ionic components in the Th–O chemical bond will be discussed in the following subsection.

3.2. Electronic structure and charge distribution

Almost all the macroscopical properties of materials, such as hardness, elasticity, and conductivity, originate from their electronic structure properties as well as the nature of the chemical bonding. Therefore it is necessary to perform the electronic structure analysis of ThO_2. The calculated band structure (left panel) and total density of states (DOS, right panel) of fluorite ThO_2 are shown in Fig. 2. The present calculated energy band gap of 4.673 eV (listed in Table 1), which is consistent with previous FLAPW (FT-LMTO) theoretical result of 4.60 (4.522) eV [10,7], indicates that ThO_2 is a typical insulator. The underestimation of band gap compared with experimental value of 6 eV [26] is due to the drawback of the exchange-correlation approximation (GGA). As a comparison, the orbital-resolved partial densities of states (PDOS) for one Th atom and two O atoms in a unit cell are also presented in Fig. 3. One can see that the low bands covering from -18.33 to -11.22 eV mainly consist of O 2s and Th 6p states which shows a clear hybridization. The high valence bands located just below the Fermi level are mainly contributed by O 2p states with a little Th 6d and 5f states and have a band width of 3.79 eV. This illustrates a significant charge transfer from Th 6d and 5f states to O 2p states. In addition, the covalency of ThO_2 comes from the mixing of Th 5f, 6d, and p states into the O 2p valence bands. As for the conduction bands, the DOS is mainly featured by Th 5f states, mixed with a little Th 6d and O 2p states and has a width of 1.78 eV.

In order to gain more insight into the bonding nature of ground state ThO_2, we also investigate the valence charge density distribution. The calculated valence charge density map of the $(1\bar{1}0)$ plane is plotted in Fig. 4. It is obvious from Fig. 4 that the charge density around Th and O ions are all near spherical distributions with slight deformation toward the direction of their nearest neighboring atoms. Furthermore, the charge density around Th and O ions is high while there is almost no valence charge in the large octahedral-hole interstitial region. This suggests remarkable ionization for thorium and oxygen ions and significant insulating property in ThO_2. In order to describe the covalency quantitatively and more clearly, we plot in the inset in Fig. 4 the line charge density distribution along the nearest Th–O bond. The charge density of Th atoms decreases to approximately equal to zero near the Th nucleus. This is due to the fact that our calculations of charge density only include the valence charge. Therefore, the arrow in the inset indicates the charge density minimum ($0.45\ \text{e/Å}^3$) along the Th–O bond. Although this value is smaller than $0.7\ \text{e/Å}^3$ for Si covalent bond, it is prominently higher than $0.05\ \text{e/Å}^3$ for Na–Cl bond in typical ionic crystal NaCl. Therefore, the Th–O bond has evident covalent property. To see the ionicity of Th–O bond, we have performed the Bader analysis [27,28]. The charge enclosed within the Bader volume is a good approximation to the total electronic charge of an atom. Note that although we have included the core charge in charge density calculations, since we do not expect variations as far as the trends are concerned, only the valence charge

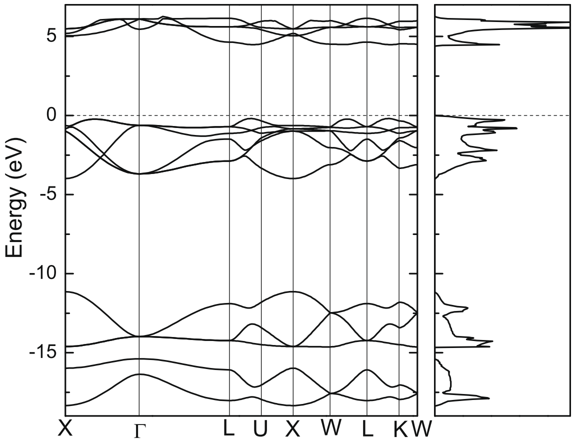

Fig. 2. Band structure (left panel) and total density of states (DOS, right panel) for ground state ThO_2 with Fermi energy level E_F taken at 0 eV as shown by the dashed lines.

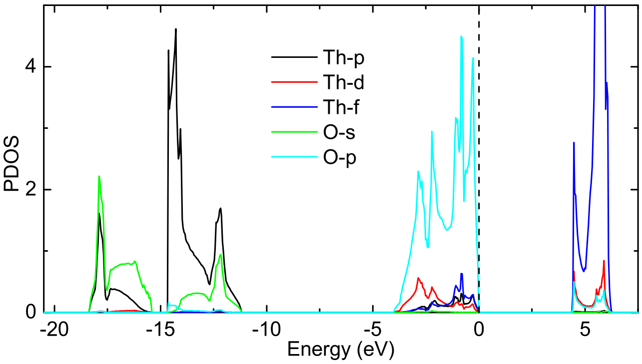

Fig. 3. Partial density of states (PDOS) for ground state ThO_2 at 0 GPa. The Fermi energy level is zero.

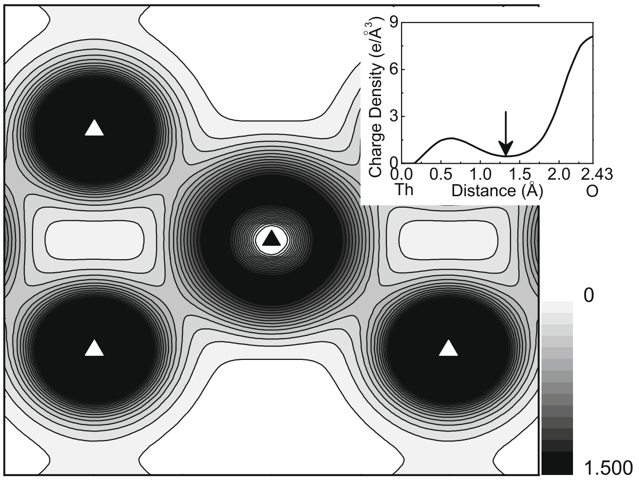

Fig. 4. Valence charge density of ThO_2 in $(1\bar{1}0)$ plane. There ▲ stands for Th, △ for O atoms. The contour lines are drawn from 0.0 to 1.5 at $0.1\ \text{e/Å}^3$ intervals. The line charge density distribution between Th atom and the nearest neighbor O atom is shown in the inset, where the arrow indicates the minimum value.

are calculated. After calculation, we find that there are 9.34 electrons around Th and 7.33 electrons around O. Therefore, about 2.66 electrons transfer from each Th atom to O atom. So, the ionicity of Th–O bond is also evident. Based on the PDOS and charge density analysis, therefore, we derive that the Th–O bond is a mixture of covalent and ionic components. From this aspect, it is now understandable that the previous full-ionic model [6] has largely underestimated the bulk modulus of ThO_2.

3.3. Phonon dispersion curve

The calculation of phonon frequencies of the crystalline structure is one of the basic aspects when considering the phase stability, phase transformations, and thermodynamics of crystalline materials. By using the Hellmann–Feynman theorem and the direct method [29], we have calculated the phonon curves along some high-symmetry directions in the Brillouin zone, together with the phonon density of states. For the phonon dispersion calculation, we used the $2 \times 2 \times 2$ fcc supercell containing 96 atoms and the $4 \times 4 \times 4$ Monkhorst–Pack k-point mesh for the Brillouin zone integration. In order to calculate the Hellmann–Feynman forces, we displace four atoms (two Th and two O atoms) from their equilibrium positions and the amplitude of all the displacements is 0.03 Å. The calculated phonon dispersion curves along the Γ–X–W–L–Γ directions are displayed in Fig. 5. The Γ–X, X–W, and L–Γ lines are along $\langle 001 \rangle$, $\langle 102 \rangle$, and $\langle 111 \rangle$ directions, respectively.

For ThO_2 in the CaF_2-structure primitive cell, there are only three atoms. Therefore, nine phonon modes exist in the dispersion relations. One can see that there is no gap between the optic modes and the acoustic branches and the LO–TO also has no splitting at Γ point. Due to the fact that thorium is heavier than oxygen atom, the vibration frequency of thorium atom is lower than that of oxygen atom. Therefore, the phonon density of states can be viewed as two parts. One is the part lower than 5.5 THz where the main contribution comes from the thorium sublattice, while the other part higher than 5.5 THz is dominated by the dynamics of the light oxygen atoms.

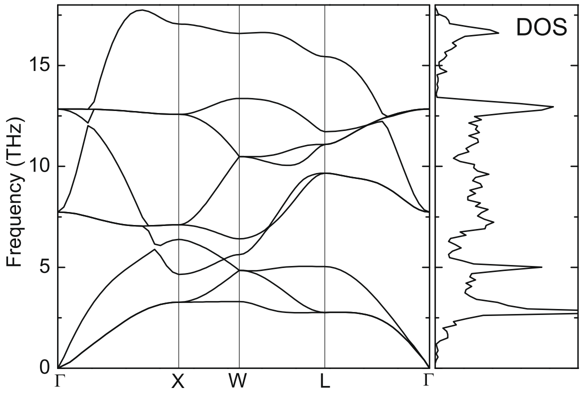

Fig. 5. Calculated phonon dispersion curves along the high-symmetry directions (left panel) and total density of states (DOS, right panel) for ground state ThO_2.

4. High pressure behavior of ThO_2

The optimized structural lattice parameters a, b, and c for the $Pnma$ phase at 0 GPa are 6.174, 3.776, and 7.161 Å, respectively, giving $V = 167.0$ Å^3. This volume, comparable to the value of 164.4 Å^3 from previous LCGTO-FF calculations [4] is prominently smaller than the equilibrium volume of 177.5 Å^3 for the $Fm\bar{3}m$ phase. Using the same method as that has been employed in our previous work on orthorhombic BeH_2 [30], we have applied the strains and calculated the elastic constants, various moduli, and Poisson's ratio υ for cotunnite-type ThO_2 at 0 GPa. The results are collected in Table 3. From Table 3 the following prominent features can be seen: (i) The orthorhombic ThO_2 at zero pressure is mechanically stable because its elastic constants satisfy the following mechanical stability criteria [31].

$$\begin{aligned}
&C_{11} > 0, C_{22} > 0, C_{33} > 0, C_{44} > 0, C_{55} > 0, C_{66} > 0,\\
&[C_{11} + C_{22} + C_{33} + 2(C_{12} + C_{13} + C_{23})] > 0,\\
&(C_{11} + C_{22} - 2C_{12}) > 0, (C_{11} + C_{33} - 2C_{13}) > 0,\\
&(C_{22} + C_{33} - 2C_{23}) > 0.
\end{aligned} \tag{13}$$

In fact, one can see from Table 3 that the calculated C_{12}, C_{23}, and C_{13} are largely smaller than C_{11}, C_{22}, and C_{33}. Therefore, the mechanical stability criteria is easily satisfied; (ii) Although the equilibrium volume of cotunnite-type ThO_2 is distinctly compressed, its bulk modulus, shear modulus, and Young's modulus are all smaller by approximately 25% than those in fluorite-type ThO_2. This intriguing behavior has also been observed in the UO_2 system [32], which, like ThO_2, will undergo a $Fm\bar{3}m \rightarrow Pnma$ phase transition. Since the 5f orbital band is occupied in UO_2, while it is almost empty in ThO_2, thus this similarity of the softening in moduli upon phase transition for the two systems is clearly unrelated with the 5f orbitals. From this aspect, we speculate that most actinide dioxides share this phase transition involved similarity. Again, we have confirmed for the $Pnma$ phase that the bulk modulus B calculated by fitting the EOS equals to that through VRH approximation. We notice that recent LCGTO-FF calculations [4] gave the bulk modulus B to be 206.8 GPa and the pressure derivative of the bulk modulus B' to be 4.94. The difference between LCGTO-FF calculations and our results can be attributed either to the type of equation of state used and/or to differences in the exchange and correlation functionals; and (iii) The Poisson's ratio υ of ThO_2 in $Pnma$ phase is nearly the same as in $Fm\bar{3}m$ phase, i.e., close to 1/3. This is understandable since the shear modulus is much smaller than the bulk modulus in the both two phases.

Now let us discuss the phase transition energetics of ThO_2. The total energies (per unit cell) of the two phases at different volumes are calculated and shown in Fig. 6. Obviously, the $Fm\bar{3}m$ phase is stable under ambient pressure while under high pressure the $Pnma$ phase becomes stable. According to the rule of common tangent of two energy curves, a phase transition at 26.5 GPa is predicted by the slope shown in the inset of Fig. 6. Besides, we also determine the phase transition pressure by comparing the Gibbs free energy as a function of pressure. At 0 K, the Gibbs free energy is equal to the enthalpy H, expressed as $H = E + PV$. Fig. 7 shows the relative enthalpies of the cotunnite phase phase with respect to the fluorite phase as a function of pressure. The crossing between the two enthalpy curves in Fig. 7 readily gives phase transition pressure of

Table 3
Calculated elastic constants, bulk modulus B, pressure derivative of the bulk modulus B', shear modulus G, Young's modulus E, Poisson's ratio υ for cotunnite-type ThO_2 at 0 GPa. Except B' and Poisson's ratio, all other values are in units of GPa.

C_{11}	C_{22}	C_{33}	C_{44}	C_{55}	C_{66}	C_{12}	C_{23}	C_{13}	B	B'	G	E	υ
299.3	256.3	235.6	37.4	54.9	84.9	73.7	95.5	104.8	148	7.8	65.9	172.2	0.307

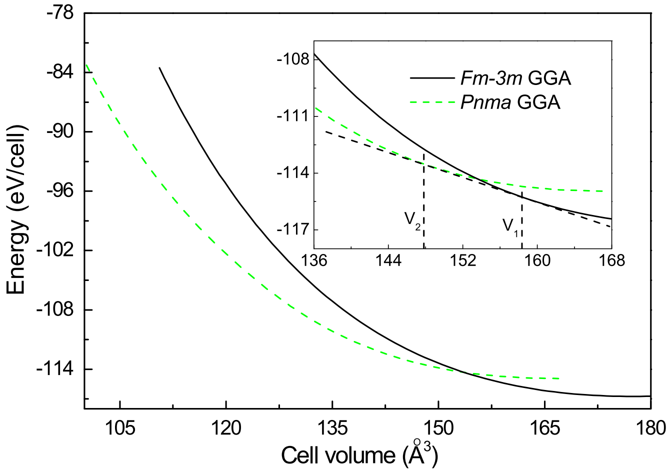

Fig. 6. Comparison of total energy vs. the cell volume for ThO_2 in $Fm\bar{3}m$ and *Pnma* phases. A phase transition at 26.5 GPa is predicted by the slope of the common-tangent-rule, as shown in the inset.

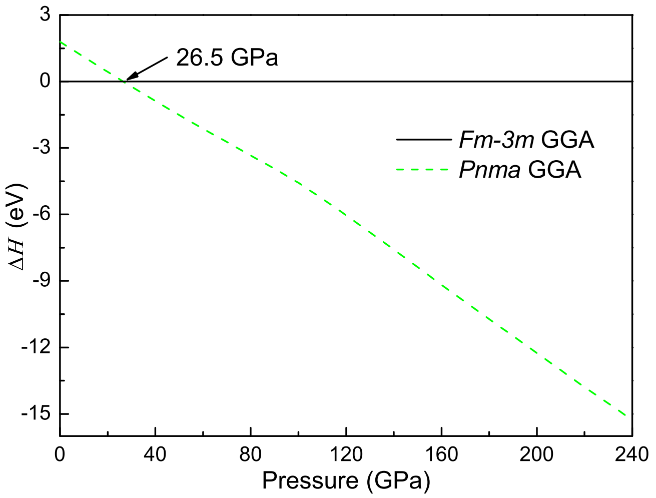

Fig. 7. Calculated enthalpy differences of *Pnma* phase with respect to $Fm\bar{3}m$ phase as a function of pressure.

26.5 GPa, which is fully consistent with the above result in terms of the common-tangent-rule. This value is well close to the experiment measurement by Idiri et al. [1] and by Jayaraman et al. [2] as ~30 GPa. Here, the minor theoretical underestimation by ~5.0 GPa is speculated to be caused by the possible existence of an energy barrier with an amplitude of Δw. To overcome this energy barrier, the external pressure P' should be larger than the conventional common-tangent-rule determined pressure P by an amount $\Delta P = P' - P$. According to the experimentally measured transition pressure P' [1] and our theoretically obtained common tangent curve in Fig. 6, we deduce the energy barrier amplitude to be ~0.06 eV (per formula unit). This value is too small to maintain the *Pnma* phase to ambient conditions, which is consistent with the fact that to date, the *Pnma* phase of ThO_2 has only be observed under high pressures.

Table 4 lists the calculated lattice parameters, atoms site at 37 GPa and the results measured by Dancausse et al. [3] at 41.2 GPa and Idiri et al. [1] at 36 GPa of *Pnma* phase. It is clear that our calculated results are on the whole in good agreement with the experimental data. The exception is that our calculated O_2 atoms site (0.474, 0.75, 0.329), in fraction coordination, is closer to the mid-position in *a* axis compared with the experimental value (0.12, 0.75, 0.27) [1]. Although it remains unclear for us how to explain this discrepancy, we can be sure that it is not caused by the choice of the exchange-correlation potential. In fact, we have found that the use of local density approximation even leads to a larger overestimation of this value. Furthermore, we fixed the coordinates of atoms at the experimental values and then calculated the total energy. Results show that this total energy is higher by about 11.46 eV (per unit cell) than that obtained in the calculation with no fixation of atoms. This confirms that our calculated results are reliable and the discrepancy need more experiments to examine.

Table 4
Calculated lattice parameters, atoms site in Wyckoff notation of orthorhombic ThO_2 at 37 GPa. Available experimental vales have been presented for comparison where the data from [3] is at 41.2 GPa and data from [1] at 36 GPa.

Property	This study	Experiment
a	5.852	5.90[a], 5.898(8)[b]
b	3.580	3.58[a], 3.600(3)[b]
c	6.840	6.81[a], 6.862(7)[b]
Volume (Å^3)	143.27	143.84[a], 145.7(3)[b]
Atoms site		
Th (4c)	(0.250, 0.25, 0.111)	(0.261, 0.25, 0.111)[b]
O_1 (4c)	(0.142, 0.25, 0.431)	(0.163, 0.25, 0.449)[b]
O_2 (4c)	(0.472, 0.75, 0.328)	(0.12, 0.75, 0.27)[b]

[a] Ref. [3].
[b] Ref. [1].

Fig. 8 shows the relative volume V/V_0 evolution with pressure for ThO_2 in both $Fm\bar{3}m$ and *Pnma* phases. For comparison, the experimental data are also shown in the figure. Clearly, our calculated P–V equation of state is well consistent with the experimental measurement for the both two phases of ThO_2. Specially, at the calculated transition pressure (26.5 GPa), our result in Fig. 8 gives that the volume collapse upon phase transition is 5.9%. This value is very close to the experimental data of 6.1% [1] with a little bit underestimation, which is obviously within the accuracy of GGA. Note that unlike the cubic $Fm\bar{3}m$ phase, in which all coordinated are completely determined at each volume due to the symmetry, the orthorhombic *Pnma* phase at each volume has two additional internal degrees of freedom that must be fully relaxed to obtain the energy minimum. Thus, we have further calculated and plotted in Fig. 9 the pressure dependence of the three lattice parameters

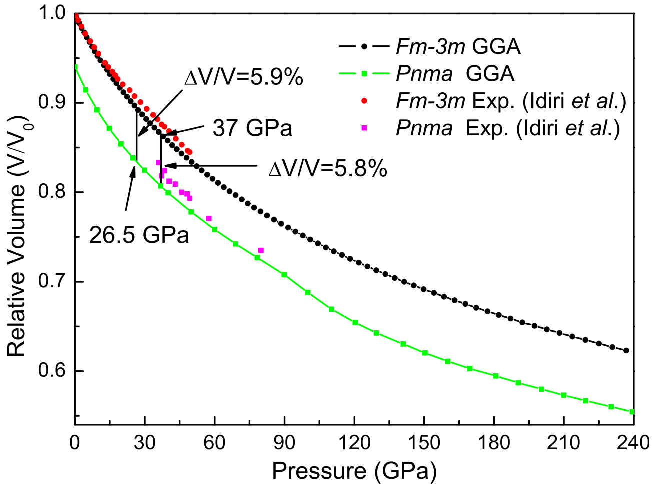

Fig. 8. Calculated compression curves of ThO_2 compared with experimental measurements. The volume collapses at our predicted phase transition point 26.5 GPa and experimental phase transition pressure 37 GPa are labeled.

(with respect to their values at calculated transition pressure 26.5 GPa) for the *Pnma* phase of ThO_2. In the experimentally reported pressure range from ~30 GPa to ~80 GPa, our calculated evolution of the relative lattice parameters in the *Pnma* phase are well consistent with the experimental observation [1]. In this pressure region, one can see from Fig. 9 that the responses of the three relative lattice parameters to the compression are anisotropic in the sense that the compression of the middle axis *a* is most rapid compared to those of the long axis *c* and small axis *b*, which vary upon compression almost in the same tendency. When the pressure becomes higher to be between 80 and 130 GPa, remarkably, it reveals in Fig. 9 that all the three relative lattice parameters undergo dramatic variations by the fact that the small axis *b* has a strong rebound and the middle *a* is collapsed. When the pressure is beyond 130 GPa, the variations of the three relative lattice parameters become smooth and approach isotropic compression. This signifies a typical isostructural transition for the *Pnma* phase of ThO_2. It should be stressed that this isostructural transition is not unique for ThO_2. A similar phenomenon has also been observed in other actinide dioxides [32].

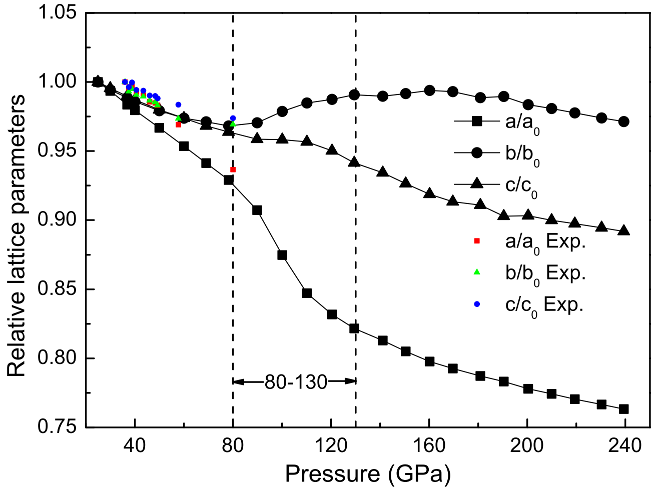

Fig. 9. Pressure behavior of the relative lattice parameters of the *Pnma* phase, where the drastic change in the relative lattice constants (region between dashed lines) indicates an isostructural transition.

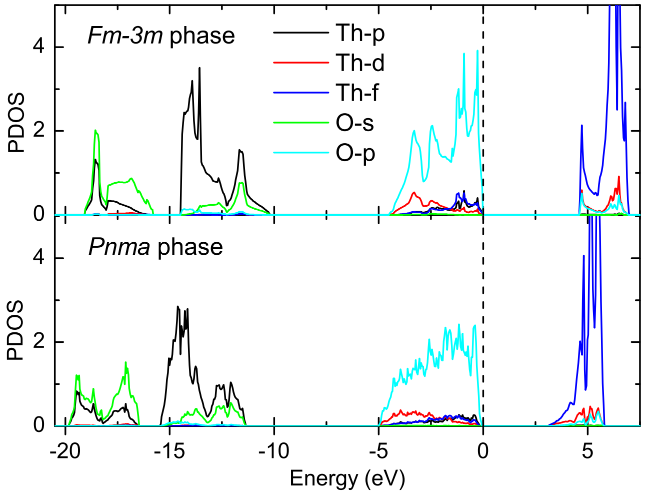

Fig. 10. Partial density of states (PDOS) for $Fm\bar{3}m$ phase (a) and *Pnma* phase (b) both at 26.5 GPa. The Fermi energy level is zero. The energy gaps of $Fm\bar{3}m$ phase and *Pnma* phase are 4.584 eV and 3.153 eV, respectively.

To see the change of electronic structure of ThO_2 under high pressure, we present in Fig. 10 the orbital-resolved PDOS for the $Fm\bar{3}m$ and *Pnma* phases at the theoretical transition pressure of 26.5 GPa. One can see that there occurs an understandable narrowing in the band gap (4.6 eV for the $Fm\bar{3}m$ phase and 3.15 eV for the *Pnma* phase). The valence and conduction bands carry a sizeable downward shift to stabilize the high-pressure *Pnma* phase. In addition, the valence and conduction bands are more widened and smooth in the *Pnma* phase. However, these changes in the electronic structure are trivial and thus cannot be associated with the exotic transition-accompanied volume collapse in ThO_2 and other actinide dioxides. Concerning the 5f electron effect, here we would like to present our viewpoint as follows. First, the 5f orbital is almost empty for both two phases of ThO_2. Therefore, the transition-accompanied volume collapse in ThO_2 is irrelevant to the 5f orbital effect. Second, in other actinide dioxides, such as PuO_2, although taking into account the 5f electronic interaction is crucial to obtain more reasonable ground state [33], this local correlation effect is not expected to play a role in explaining the transition-accompanied volume collapse in these 5f-occupied actinide dioxides. The reason is simply because that inclusion of 5f electronic localization will weaken the binding of cations and anions, causing an increase instead of a decrease in the volume of system. Therefore, the phenomenon of volume collapse during high-pressure phase transition of the actinide dioxides is mainly attributed to the ionic (instead of electronic) response to the external compression.

5. Conclusion

In summary, the ground-state properties as well as the high pressure behavior of ThO_2 were studied by means of the first-principles DFT-GGA method. The elastic constants and their derived moduli and Poisson's ratio were calculated for both the ambient $Fm\bar{3}m$ and the high-pressure *Pnma* phases of ThO_2 and were shown to agree well with recent reliable experiments. Based on these results, the mechanical stability of the *Pnma* phase at zero pressure was predicted. The hardness, lattice vibration dynamics, and the Th–O chemical bond of the ambient phase were calculated and analyzed in order to support the practical application of ThO_2. We showed that the Th–O bond displays a mixed ionic/covalent character. Here the ionicity is mainly featured by charge transfer from Th 6d/5f states to O 2p states, while the covalency is manifested by hybridization of thorium 5f, 6d and p states into oxygen 2p states. This mixed ionic/covalent feature makes ThO_2 a hard material, with its hardness calculated in this paper to be ~22 GPa. As another main task, we studied phase transition of ThO_2 under high pressure. Our calculated $Fm\bar{3}m \rightarrow Pnma$ transition pressure is 26.5 GPa, according well with recent experimental results of ~30 GPa. Our calculated transition-accompanied volume collapse of 5.9% is also in good agreement with the experimental data of 6.1%. At higher pressure, we further found that an isostructural transition occurs between 80 and 130 GPa for the *Pnma* phase, which is to be experimentally verified in future.

Acknowledgment

This work was supported by the Foundations for Development of Science and Technology of China Academy of Engineering Physics under Grant No. 2009B0301037 and NCET of the Ministry of Education of China (Grant No. NCET-08-0883).

References

[1] M. Idiri, T. Le Bihan, S. Heathman, J. Rebizant, Phys. Rev. B 70 (2004) 014113.
[2] A. Jayaraman, G.A. Kourouklis, L.G. Van Uitert, Pramana 30 (1988) 225.

[3] J.P. Dancausse, E. Gering, S. Heathman, U. Benedict, High Pressure Res. 2 (1990) 381.
[4] J.C. Boettger, Int. J. Quantum. Chem. 109 (2009) 3564.
[5] P.J. Kelly, M.S.S. Brooks, J. Chem. Soc. Faraday Trans. 2 (83) (1987) 1189.
[6] J.H. Harding, P.J.D. Lindan, N.C. Pyper, J. Phys.: Condens. Matter 6 (1994) 6485.
[7] J. Staun Olsen, L. Gerward, V. Kanchana, G. Vaitheeswaran, J. Alloys Compd. 381 (2004) 37.
[8] S. Li, R. Ahuja, B. Johansson, High Pressure Res. 22 (2002) 471.
[9] V. Kanchana, G. Vaitheeswaran, A. Svane, A. Delin, J. Phys.: Condens. Matter 18 (2006) 9615.
[10] I.R. Shein, K.I. Shein, A.L. Ivanovskii, J. Nucl. Mater. 361 (2007) 69.
[11] Y. Yun, P.M. Oppeneer, H. Kim, K. Park, Acta Mater. 57 (2009) 1655.
[12] G. Kresse, J. Furthmüller, Phys. Rev. B 54 (1996) 11169.
[13] J.P. Perdew, K. Burke, Y. Wang, Phys. Rev. B 54 (1996) 16533.
[14] P.E. Blöchl, Phys. Rev. B 50 (1994) 17953.
[15] H.J. Monkhorst, J.D. Pack, Phys. Rev. B 13 (1972) 5188.
[16] F. Birch, Phys. Rev. 71 (1947) 809.
[17] J.F. Nye, Physical Properties of Crystals, Their Representation by Tensors and Matrices, Oxford Press, 1957 (Chapter. VIII).
[18] J.H. Westbrook, R.L. Fleischer (Eds.), Intermetallic Compounds: Principles and Practice, Principles, vol. I, Wiley, London, 1995, p. 195 (Chapter 9).
[19] P.M. Macedo, W. Capps, J.B. Watchman, J. Am. Ceram. Soc. 47 (1964) 651.
[20] W. Voigt, Lehrburch der Kristallphysik, Teubner, Leipzig, 1928.
[21] A. Reuss, Z. Angew, Math. Mech. 9 (1929) 49.
[22] R. Hill, Phys. Soc. Lond. 65 (1952) 350.
[23] J.P. Watt, J. Appl. Phys. 50 (1979) 6290.
[24] P. Ravindran, L. Fast, P.A. Korzhavyi, B. Johansson, J. Wills, O. Eriksson, J. Appl. Phys. 84 (1998) 4891.
[25] A. Simunek, J. Vackar, Phys. Rev. Lett. 96 (2006) 085501.
[26] A.A. Sviridova, N.V. Suikovskaya, Opt. Spectrosk. 22 (1965) 940.
[27] R.F.W. Bader, Atoms in Molecules: A Quantum Theory, Oxford University Press, New York, 1990.
[28] W. Tang, E. Sanville, G. Henkelman, J. Phys.: Condens. Matter 21 (2009) 084204.
[29] K. Parlinski, Z.Q. Li, Y. Kawazoe, Phys. Rev. Lett. 78 (1997) 4063.
[30] B.T. Wang, P. Zhang, H.L. Shi, B. Sun, W.D. Li, 2009. aiXiv:0905.4589v1 (cond-mat.mtrl-sci).
[31] J.F. Nye, Physical Properties of Crystals, Oxford University Press, 1985.
[32] H.Y. Geng, Y. Chen, Y. Kaneta, M. Kinoshita, Phys. Rev. B 75 (2007) 054111.
[33] B. Sun, P. Zhang, X.G. Zhao, J. Chem. Phys. 128 (2008) 084705.